

# HELICITY AMPLITUDES AND SUM RULES FOR REAL AND VIRTUAL PHOTONS

L. TIATOR

*Institut für Kernphysik, Johannes Gutenberg-Universität, J. J. Becher-Weg 45,  
D-55099 Mainz, Germany*

*E-mail: tiator@kph.uni-mainz.de*

Results of the recently developed unitary isobar model (MAID) are presented for helicity amplitudes, spin asymmetries, structure functions and relevant sum rules for real and virtual photons in the resonance region. Our evaluation of the energy-weighted integrals is in good agreement for the proton but shows big discrepancies for the neutron.

## 1 Introduction

The spin structure of the nucleon in the resonance region is of particular interest to understand the rapid transition from resonance dominated coherent processes to incoherent processes of deep inelastic scattering (DIS) off the constituents. Here we present the results of the recently developed unitary isobar model (MAID)<sup>1</sup> for the spin asymmetries, structure functions and relevant sum rules in the resonance region. This model describes the presently available data for single-pion photo- and electroproduction up to a total  $cm$  energy  $W_{\max} = 2$  GeV and for  $Q^2 \leq 4$  (GeV/c)<sup>2</sup>. It is based on effective Lagrangians for Born terms and vector meson exchange (background) and resonance contributions modeled by Breit-Wigner functions. All major resonances below  $W = 1700$  MeV are included. The respective multipoles are constructed in a gauge-invariant and unitary way for each partial wave. The eta production is included in a similar way<sup>2</sup>, while the contribution of more-pion and higher channels is modeled by comparison with the total cross sections and simple phenomenological assumptions.

## 2 Formalism

The differential cross section for exclusive electroproduction of mesons from polarized targets using polarized electrons, e.g.  $\vec{p}(\vec{e}, e'\pi^0)p$  can be parametrized in terms of 18 response functions<sup>3</sup>, a total of 36 is possible if in addition also the recoil polarization is observed. Due to the azimuthal symmetry most of them vanish by integration over the angle  $\phi$  and only 5 total cross sections remain. The differential cross section for the electron is

then given by

$$\frac{d\sigma}{d\Omega dE'} = \Gamma\sigma(\nu, Q^2), \quad (1)$$

$$\sigma = \sigma_T + \epsilon\sigma_L + P_y\sqrt{2\epsilon(1+\epsilon)}\sigma_{LT} + hP_x\sqrt{2\epsilon(1-\epsilon)}\sigma_{LT'} + hP_z\sqrt{1-\epsilon^2}\sigma_{TT'}, \quad (2)$$

where  $\Gamma$  is the flux of the virtual photon field and the  $\sigma_i$ ,  $i = L, T, LT, LT', TT'$ , are functions of the *lab* energy of the virtual photon  $\nu$  and the squared four-momentum transferred  $Q^2$ . These response functions can be separated by varying the transverse polarization  $\epsilon$  of the virtual photon as well as the polarizations of the electron ( $h$ ) and proton ( $P_z$  parallel,  $P_x$  perpendicular to the virtual photon, in the scattering plane and  $P_y$  perpendicular to the scattering plane). In particular,  $\sigma_T$  and  $\sigma_{TT'}$  can be expressed in terms of the total cross sections for excitation of hadronic states with spin projections  $3/2$  and  $1/2$ :  $\sigma_T = (\sigma_{3/2} + \sigma_{1/2})/2$  and  $\sigma_{TT'} = (\sigma_{3/2} - \sigma_{1/2})/2$ .

Here we use Hand's notation with the equivalent photon *cm* energy  $K = (W^2 - m^2)/(2W)$  for the virtual photon flux. Correspondingly, the phase space factors of the cross sections are given by  $q/K$ , where  $q$  is the pion momentum in the *cm*.

In inclusive electron scattering  $\vec{e} + \vec{N} \rightarrow X$ , only 4 cross sections  $\sigma_T, \sigma_L, \sigma_{LT'}$  and  $\sigma_{TT'}$  appear, the fifth cross section,  $\sigma_{LT}$ , vanishes due to unitarity when all open channels are summed up. The individual channels, however, give finite contributions.

The Gerasimov-Drell-Hearn (GDH) sum rule is only derived for real photons. It is based on unitarity and low-energy theorems and the assumption of the convergence of an unsubtracted dispersion relation,

$$I_{GDH} = \frac{m^2}{8\pi^2\alpha} \int_{\nu_0}^{\infty} (\sigma_{1/2} - \sigma_{3/2}) \frac{d\nu}{\nu} = -\frac{\kappa^2}{4}. \quad (3)$$

This sum rule is often presented without the leading factor in front of the integral, the numerical conversion is  $8\pi^2\alpha/m^2 = 254.8\mu b$ .

It can be generalized in various ways. Three forms often used in the literature are summing up only contributions from  $\sigma_{TT'}$  with no longitudinal terms,

$$I_{GDH}^{(a)}(Q^2) = \frac{m^2}{8\pi^2\alpha} \int_{\nu_0}^{\infty} (1-x)(\sigma_{1/2} - \sigma_{3/2}) \frac{d\nu}{\nu}, \quad (4)$$

$$I_{GDH}^{(b)}(Q^2) = \frac{m^2}{8\pi^2\alpha} \int_{\nu_0}^{\infty} \frac{K}{|\vec{k}_\gamma|} (\sigma_{1/2} - \sigma_{3/2}) \frac{d\nu}{\nu}, \quad (5)$$

$$I_{GDH}^{(c)}(Q^2) = \frac{m^2}{8\pi^2\alpha} \int_{\nu_0}^{\infty} (\sigma_{1/2} - \sigma_{3/2}) \frac{d\nu}{\nu} . \quad (6)$$

The factor  $K/|\vec{k}_\gamma|$  can also be expressed as  $(1-x)/\sqrt{1+\gamma^2}$ . The relations between the  $\sigma_i$  and the quark structure functions  $g_1$  and  $g_2$  can be read off the following equations, which define further possible generalizations of the GDH integral<sup>4</sup> and the Burkhardt-Cottingham (BC) sum rule<sup>5</sup>, which in addition also include longitudinal-transverse interference terms,

$$\begin{aligned} I_1(Q^2) &= \frac{2m^2}{Q^2} \int_0^{x_0} g_1(x, Q^2) dx \\ &= \frac{m^2}{8\pi^2\alpha} \int_{\nu_0}^{\infty} \frac{1-x}{1+\gamma^2} (\sigma_{1/2} - \sigma_{3/2} - 2\gamma\sigma_{LT'}) \frac{d\nu}{\nu} , \end{aligned} \quad (7)$$

$$\begin{aligned} I_2(Q^2) &= \frac{2m^2}{Q^2} \int_0^{x_0} g_2(x, Q^2) dx \\ &= \frac{m^2}{8\pi^2\alpha} \int_{\nu_0}^{\infty} \frac{1-x}{1+\gamma^2} \left( \sigma_{3/2} - \sigma_{1/2} - \frac{2}{\gamma}\sigma_{LT'} \right) \frac{d\nu}{\nu} , \end{aligned} \quad (8)$$

$$\begin{aligned} I_3(Q^2) &= \frac{2m^2}{Q^2} \int_0^{x_0} (g_1(x, Q^2) + g_2(x, Q^2)) dx \\ &= -\frac{m^2}{4\pi^2\alpha} \int_{\nu_0}^{\infty} \frac{1-x}{Q} \sigma_{LT'} d\nu = I_1 + I_2 , \end{aligned} \quad (9)$$

where  $\gamma = Q/\nu$  and  $x = Q^2/2m\nu$  the Bjorken scaling variable, with  $x_0$  ( $\nu_0$ ) referring to the inelastic threshold of one-pion production. Since  $\sigma_{LT'} = \mathcal{O}(Q)$ , the real photon limit of the integral  $I_1$  is given by the GDH sum rule  $I_1(0) = I_{GDH}(0) = -\kappa_N^2/4$ , with  $\kappa_N$  the anomalous magnetic moment of the nucleon. At large  $Q^2$  the structure functions should depend only on  $x$ , i.e.  $I_1 \rightarrow 2m\Gamma_1/Q^2$  with  $\Gamma_1 = \int g_1(x)dx = \text{const}$ . In the case of the proton, all experiments for  $Q^2 > 1\text{GeV}^2$  yield  $\Gamma_1 > 0$ . Therefore, a strong variation of  $I_1(Q^2)$  with a zero-crossing at  $Q^2 < 1\text{ GeV}^2$  is required in order to reconcile the GDH sum rule with the measurements in the DIS region. The  $I_2$  integral of Eq. (8) is constrained by the BC sum rule, which requires that the inelastic contribution for  $0 < x < x_0$  equals the negative value of the elastic contribution, i.e.

$$I_2(Q^2) = \frac{2m^2}{Q^2} \int_0^{x_0} g_2(x, Q^2) dx = \frac{1}{4} \frac{G_M(Q^2) - G_E(Q^2)}{1 + Q^2/4m^2} G_M(Q^2) , \quad (10)$$

where  $G_M$  and  $G_E$  are the magnetic and electric Sachs form factors respectively. At large  $Q^2$  the integral vanishes as  $Q^{-10}$ , while at the real photon

limit  $I_2(0) = \kappa_N^2/4 + e_N\kappa_N/4$ , the two terms on the right hand side corresponding to the contributions of  $\sigma_{TT'}$  and  $\sigma_{LT'}$  respectively. Finally, Eq. (9) defines an integral  $I_3(Q^2)$  as the sum of  $I_1(Q^2)$  and  $I_2(Q^2)$  and is given by the unweighted integral over the longitudinal-transverse interference cross section  $\sigma_{LT'}$ . At the real photon point this integral is given by the GDH and BC sum rules,  $I_3(0) = e_N\kappa_N/4$ . In particular this vanishes for the neutron target.

### 3 Unitary Isobar Model

Our calculation for the response functions  $\sigma_i$  is based on the Unitary Isobar Model (UIM) for one-pion photo- and electroproduction of Ref.<sup>1</sup>, accessible in the internet as the MAID program. The model is constructed with effective Lagrangians for Born terms, vector meson exchange in the  $t$  channel (background), and the dominant resonances up to the third resonance region are modeled using Breit-Wigner functions with energy-dependent widths. For each partial wave the multipoles satisfy gauge invariance and unitarity. As in any realistic model a special effort is needed to describe the  $s$ -channel multipoles  $S_{11}$  and  $S_{31}$ . Even close at threshold these multipoles pick up sizeable imaginary parts that cannot be explained by nucleon resonances. In fact the  $S_{11}(1535)$ ,  $S_{11}(1650)$  and the  $S_{31}(1620)$  play only a minor role for the complex phase of the  $E_{0+}$  multipoles even at higher energies. The main effect arises from pion rescattering. This we can take into account by  $K$ -matrix unitarization. Furthermore we introduce a gauge invariant contact term proportional to the anomalous magnetic moment of the nucleon  $\kappa_N$ ,

$$j_\kappa^\mu = \frac{ieg}{2m} \kappa_N F(q_0^2) \frac{\sigma^{\mu\nu} k_\nu}{2m} \gamma_5. \quad (11)$$

The form factor  $F(q_0^2)$ ,  $q_0$  being the asymptotic pion momentum, vanishes at threshold, consistent with chiral symmetry, but gives rise to a cancellation of unphysically high momentum components in the Born terms at high energies.

Due to unitarity each partial wave has to fulfill Watson's theorem,

$$\begin{aligned} t_{\gamma,\pi}^\alpha &= t_{\gamma,\pi}^\alpha(\text{background}) + t_{\gamma,\pi}^\alpha(\text{resonances}) \\ &= \pm |t_{\gamma,\pi}^\alpha| e^{i\delta_{\pi N}^\alpha}. \end{aligned} \quad (12)$$

In an isobar model this condition has to be constructed explicitly. In Maid98 the background is real (except for the S-waves) and a phase is added to the resonance. In Maid2000 both background and resonance contributions are unitarized separately for all partial waves up to  $l = 3$  in the following way

$$t_{\gamma,\pi}^\alpha = t_{\gamma,\pi}^\alpha(\text{Born} + \omega, \rho)(1 + i t_{\pi N}^I) + t_{\gamma,\pi}^\alpha(\text{resonances}) e^{i\Psi^\alpha}. \quad (13)$$

The UIM is able to describe the single-pion electroproduction channel quite well. However, at higher energies the contributions from other channels become increasingly important. In the structure functions  $\sigma_T$  and  $\sigma_{TT'}$  we account for the  $\eta$  and the multi-pion production contributions extracting the necessary information from the existing data for the total cross section<sup>8</sup>. In Fig. 1 we show the individual channels for the total helicity dependent cross sections  $\sigma_{1/2}$ ,  $\sigma_{3/2}$ ,  $\sigma_T$  and  $\Delta\sigma = 2\sigma_{TT'}$  at  $Q^2 = 0$ . Due to the non-regularized Born terms in the  $1\pi$  channels the cross sections start to rise again at energies  $W > 1.8$  GeV. However, because of the energy weighting, the effect is negligible for the integrals.

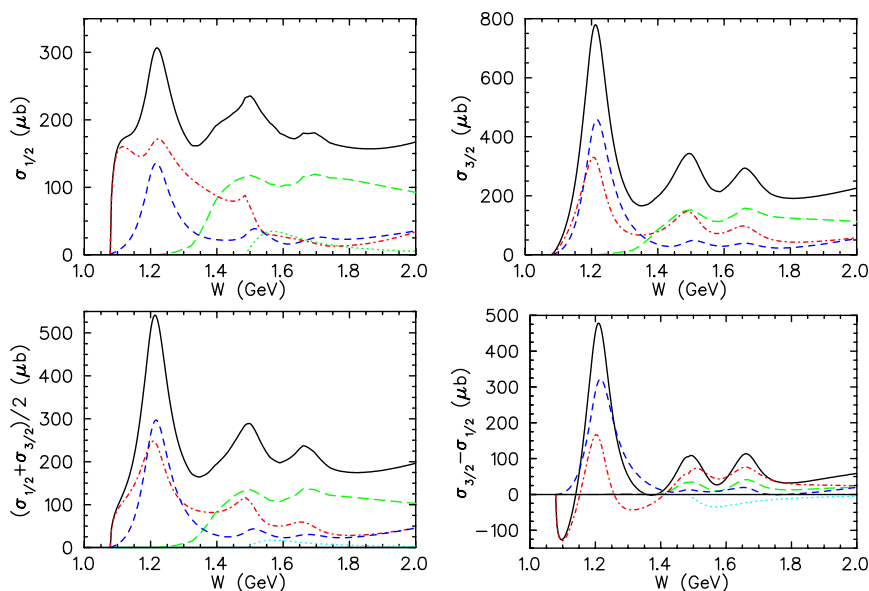


Figure 1. Helicity dependent cross sections for photoproduction on the proton target. The dashed, dash-dotted, long dashed and dotted lines show our calculations for  $\pi^0$ ,  $\pi^+$ , two-pion and the  $\eta$  cross sections, respectively. The solid curves give the total photoabsorption and contain the sum of all.

## 4 Integrals

### 4.1 Results for Real Photons

In Tab. 1 we show our results for the GDH integral and the forward spin polarizability over the lab energy range of 200-450 MeV together with the

latest Mainz data<sup>9</sup>. In comparison with the results of the dispersion theoretical partial wave analysis HDT<sup>12</sup> and the SAID solution SM99K<sup>11</sup> our MAID results agree very well with the experiment. The additional information on the individual channels, however, offers interesting insights in the different calculations, especially the  $\pi^+$  result of SAID for  $\gamma_0$  is a factor 3 larger than MAID and about a factor 2 above the data. The reason is the enhanced sensitivity of background contributions in the  $\pi^+$  channel, especially the S-wave near threshold. Tab. 2 shows the GDH integral over the full energy range

Table 1. Contributions to the GDH integral  $I = \int_{200}^{450} (\sigma_{1/2} - \sigma_{3/2})/\nu d\nu$  and to the forward spin polarizability of the proton  $\gamma_0 = 1/4\pi^2 \int_{200}^{450} (\sigma_{1/2} - \sigma_{3/2})/\nu^3 d\nu$  for photon *lab* energies of 200-450 MeV.

$I(\mu b)$	Mainz exp. <sup>9</sup>	SM99K <sup>11</sup>	HDT <sup>12</sup>	MAID <sup>1</sup>
$\pi^0 p$	$-124 \pm 11$	-132	-144	-136
$\pi^+ n$	$-33 \pm 3$	-55	-26	-23
total	$-157 \pm 11$	-187	-170	-159
$\gamma_0(10^{-4} fm^4)$				
$\pi^0 p$	$-1.2 \pm 0.3$	-1.34	-1.48	-1.40
$\pi^+ n$	$-0.23 \pm 0.04$	-0.54	-0.19	-0.17
total	$-1.4 \pm 0.3$	-1.88	-1.67	-1.57

Table 2. Contributions to the GDH integral for proton and neutron: Sum rules  $-2\pi^2 \alpha \kappa_N/m^2$  (sr), Mainz experiment<sup>13</sup> in the energy interval of 200-800 MeV, MAID  $1\pi$  contributions, eta production<sup>2</sup>, reggeized  $2\pi$  contributions (Born terms and  $D_{13}(1520)$  resonance)<sup>10</sup>.

$I(\mu b)$	sr	exp.	$\gamma, \pi^0$	$\gamma, \pi^\pm$	$\gamma, \eta$	$\gamma, \pi\pi B$	$\gamma, \pi\pi D$	sum
prot.	-205	$-216 \pm 6$	-150	-21	+15	-30	-15	-201
neut.	-233	—	-154	+30	+10	-35	-15	-164

up to  $W_{max} = 2$  GeV. The preliminary experimental result is obtained only from measurements at Mainz and covers the energy range from 200 to 800 MeV photon *lab* energy. However, our theoretical calculations indicate a very close cancellation between the low energy contribution from threshold up to 200 MeV ( $30 \mu b$ ) and of energies above 800 MeV ( $-34 \mu b$ ). For our detailed comparison we included recent calculations of reggeized  $\pi\pi$  photoproduction by Holvoet and Vanderhaeghen<sup>10</sup> that include  $\gamma, \pi\Delta$  Born terms and additional  $D_{13}(1520)$  excitations. This  $2\pi$  contribution to the GDH integral is

about twice as large as compared to our simple phenomenological multi-pion parametrization used for finite  $Q^2$ .

Our calculation that also include very recent Regge-type calculations for two-pion photoproduction<sup>10</sup> shows a very good agreement with the sum rule for the proton target but also exhibits a big deviation for the neutron target. However, on the neutron target the photoproduction information is rather limited above the  $\Delta$  region and it has to be further investigated if the high-energy region is perhaps more important than for the proton target. Furthermore, for both nucleon targets high energy contributions beyond the two-pion production have to be studied that make a very big contribution in deep inelastic scattering at finite  $Q^2 > 1\text{GeV}^2$ . In Tab. 3 we give the individ-

Table 3. Contributions to the forward spin polarizability for proton and neutron: Mainz experiment<sup>13</sup> in the energy interval of 200-800 MeV, experimental value plus threshold and high energy region, MAID  $1\pi$  contributions, eta plus multi-pion production. Values are given in units of  $10^{-4} fm^4$

$\gamma_0$	exp	exp +	$\gamma, \pi^0$	$\gamma, \pi^\pm$	$\gamma, \eta +$	sum
proton	$-1.71 \pm 0.09$	$-0.78 \pm 0.09$	-1.47	0.80	-0.01	-0.68
neutron	—	—	-1.50	1.66	-0.01	0.15

ual contributions to the forward spin polarizability  $\gamma_0$  in the resonance region,  $W_{thr} < W < 2$  GeV. Due to the strong energy weighting  $1/\nu^3$ , the high-energy contribution beyond  $\nu = 800\text{MeV}$  is practically negligible. On the other side, the threshold region below  $\nu = 200\text{MeV}$  is strongly enhanced in comparison to the GDH integral. To compare with the value of the Mainz experiment we have added the low-energy contribution to the measured value and have obtained an experimental value for the full energy range. In particular, the correction is very much dominated by low-energy constraints, therefore the estimate is rather model-independent.

#### 4.2 Results for Virtual Photons

In Fig. 2 and Fig. 3 we give our predictions for the integrals  $I_{GDH}(Q^2)$ ,  $I_1(Q^2)$ ,  $I_2(Q^2)$  and  $I_3(Q^2)$  in the resonance region, i.e. integrated up to  $W_{max} = 2$  GeV for the proton and neutron targets. A comparison of the 3 different forms, defined in Eqs. 4, 5, 6 show significantly different slopes at  $Q^2 = 0$  and quite different zero positions, where the GDH integral crosses from negative values observed for real photons to positive values known from deep inelastic scattering. In the case of the integral  $I_1$ , our model is able to generate the expected drastic change in the helicity structure at low  $Q^2$ . We find a zero-

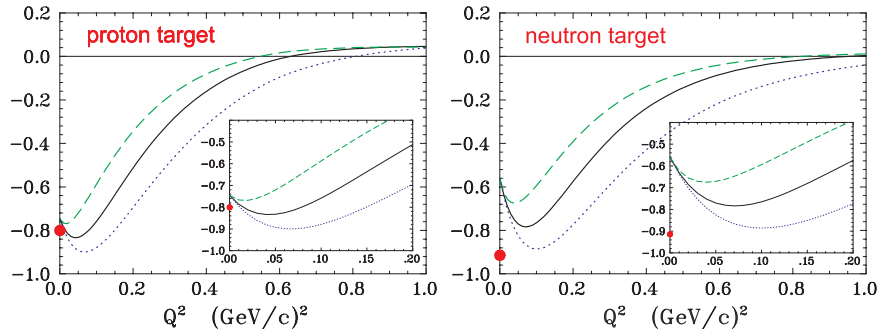


Figure 2. Generalized GDH integrals  $I_{GDH}(Q^2)$  for 3 different definitions used in the literature. The full, dashed and dotted lines show the integrals (a), (b), (c) in the notation of Eqs. 4, 5, 6, respectively. The integrals are evaluated up to  $W = 2$  GeV and include  $1\pi + \eta + n\pi$  contributions.

crossing at  $Q^2 = 0.75$   $(\text{GeV}/c)^2$  if we include only the one-pion contribution. This value is lowered to  $0.52$   $(\text{GeV}/c)^2$  and  $0.45$   $(\text{GeV}/c)^2$  when we include the  $\eta$  and the multi-pion contributions respectively. The SLAC analysis of the proton yields  $I_1 = 0.1 \pm 0.06$  at  $Q^2 = 0.5$   $(\text{GeV}/c)^2$ , while our result at this point is only slightly positive. For the neutron our calculation is fully consistent within the SLAC analysis at  $Q^2 = 0.5$   $(\text{GeV}/c)^2$  in contrast to the large discrepancy observed at  $Q^2 = 0$ , see Tab. 2.

Comparing with the generalizations of the GDH sum rule in Fig. 2 and Fig. 3, it can be seen that the slope at  $Q^2 = 0$  and the existence of a minimum for small  $Q^2$  depends on the inclusion of the longitudinal contributions, i.e. the minimum disappears when  $\sigma_{LT'}$  is added. Concerning the integral  $I_2$ , our full result is in good agreement with the prediction of the BC sum rule. The deviation is within 10 % and should be attributed to contributions beyond  $W_{\text{max}} = 2$  GeV and the uncertainties in our calculation for  $\sigma_{LT'}$ . As seen in Eq. (9) the integral  $I_3$  depends only on this  $\sigma_{LT'}$  contribution. From the sum rule result a value of  $e_N \kappa_N / 4$  is expected at  $Q^2 = 0$ , i.e. 0.45 for the proton and zero for the neutron target. While our value arising entirely from the  $1\pi$  channel (0.59) gets relatively close to the sum rule result for the proton, in the neutron case this sum rule is heavily violated (0.78). So far it is not clear where such a large negative contribution should arise for the neutron target in order to cancel the  $1\pi$  contribution. Either it is due to the high-energy tail that may converge rather slowly for the unweighted integral  $I_3$ , or the multi-pion channels could contribute in such a way, while the eta channel is



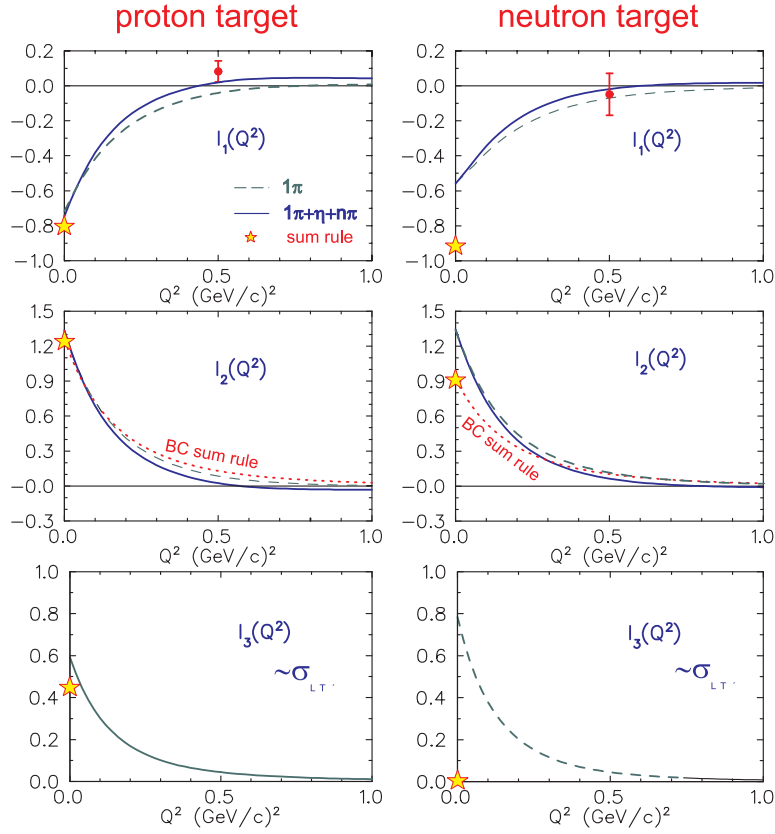


Figure 3. Generalized GDH integrals  $I_{1,2,3}(Q^2)$  for the proton and the neutron integrated up to  $W_{\max} = 2$  GeV. The dashed lines show the contributions from the  $1\pi$  channel while the full lines include  $1\pi + \eta + n\pi$ . The dotted line for  $I_2$  is the  $BC$  sum rule prediction of Ref.<sup>5</sup>. The data is from SLAC, Ref.<sup>14</sup>. The stars show the sum rules at  $Q^2 = 0$

very unlikely. In any case a careful study of the multi-pion contribution for both proton and neutron targets will be very helpful, in particular one can expect longitudinal contributions from the non-resonant background.

## 5 Summary

In summary, we have applied our recently developed unitary isobar model for pion electroproduction to calculate generalized GDH integrals and the

BC sum rule for both proton and neutron targets. Our results indicate that both the experimental analysis and the theoretical models have to be quite accurate in order to fully describe the helicity structure of the cross section in the resonance region.

While our results agree quite well for the GDH and BC sum rules for the proton, we find substantial deviations for the neutron target, in particular the sum rule  $I_3(0) \equiv I_1(0) + I_2(0) = 0$  is heavily violated by the contribution from the single-pion channel which is even larger than in the case of the proton. Concerning the theoretical description, the treatment of the multi-pion channels has to be improved with more refined models. On the experimental side, the upcoming results from measurements with real and virtual photons from ELSA, GRAAL and JLab hold the promise to provide new precision data in the resonance region.

### Acknowledgments

We would like to thank M. Vanderhaeghen for the contributions to the  $\pi\pi$  channels and J. Arends for the information on the experimental data analysis. This work was supported by the Deutsche Forschungsgemeinschaft (SFB 443).

### References

1. D. Drechsel, O. Hanstein, S.S. Kamalov and L. Tiator, Nucl. Phys. A **645**, 145 (1999); <http://www.kph.uni-mainz.de/MAID/>
2. G. Knöchlein, D. Drechsel, L. Tiator, Z. Phys. A **352**, 327 (1995).
3. D. Drechsel and L. Tiator, Journ. Phys. G **18**, 449 (1992).
4. S.B. Gerasimov, Sov. J. Nucl. Phys. **2**, 430 (1966); S.D. Drell and A.C. Hearn, Phys. Rev. Lett. **16**, 908 (1966).
5. H. Burkhardt and W.N. Cottingham, Ann. Phys. (N.Y.) **56**, 453 (1970).
6. C. Mertz et al, nucl-ex/9902012.
7. V.V. Frolov et al., Phys. Rev. Lett. **82**, 45 (1999).
8. D. Drechsel, S.S. Kamalov, G. Krein, and L. Tiator, Phys. Rev. D **59**, 094021 (1999).
9. GDH Collaboration, J. Ahrens et al, Phys. Rev. Lett. **84**, 5950 (2000).
10. H. Holvoet, M. Vanderhaeghen, in progress.
11. R.A. Arndt, I.I. Strakovsky and R.L. Workman, Phys. Rev. C **53**, 430 (1996) (SM99K solution of the GWU analysis).
12. O. Hanstein, D. Drechsel, and L. Tiator, Nucl. Phys. A **632**, 561 (1998).
13. P. Pedroni, contribution to this GDH2000 workshop.
14. E143 Collaboration, K. Abe et al., Phys. Rev. D **58**, 112003 (1998).

